JACS
JOURNAL OF THE AMERICAN CHEMICAL SOCIETY
Article
pubs.acs.org/JACS

Synthesis of NBN-Type Zigzag-Edged Polycyclic Aromatic Hydrocarbons: 1,9-Diaza-9a-boraphenalene as a Structural Motif

Xinyang Wang,[†] Fan Zhang,*[,†] Karl Sebastian Schellhammer,[‡,§] Peter Machata,[∥] Frank Ortmann,[‡] Gianaurelio Cuniberti,[‡,§] Yubin Fu,[§] Jens Hunger,[§] Ruizhi Tang,[†] Alexey A. Popov,[∥] Reinhard Berger,[§] Klaus Müllen,[⊥] and Xinliang Feng*[,†,§]

[†]School of Chemistry and Chemical Engineering, State Key Laboratory of Metal Matrix Composites, Shanghai Jiao Tong University, Shanghai 200240, P. R. China

[‡]Institute for Materials Science, Max Bergmann Center of Biomaterials and Dresden Center for Computational Materials Science, Technische Universität Dresden, 01062 Dresden, Germany

[§]Center for Advancing Electronics Dresden (cfaed) and Department of Chemistry and Food Chemistry, Technische Universität Dresden, 01062 Dresden, Germany

[∥]Center of Spectroelectrochemistry, Department of Electrochemistry and Conducting Polymers, Leibniz Institute for Solid State and Materials Research, 01069 Dresden, Germany

[⊥]Max Planck Institute for Polymer Research, Ackermannweg 10, 55128 Mainz, Germany

Supporting Information

ABSTRACT: A novel class of dibenzo-fused 1,9-diaza-9a-boraphenalenes featuring zigzag edges with a nitrogen−boron−nitrogen bonding pattern named NBN-dibenzophenalenes (NBN-DBPs) has been synthesized. Alternating nitrogen and boron atoms impart high chemical stability to these zigzag-edged polycyclic aromatic hydrocarbons (PAHs), and this motif even allows for postsynthetic modifications, as demonstrated here through electrophilic bromination and subsequent palladium-catalyzed cross-coupling reactions. Upon oxidation, as a typical example, NBN-DBP **5a** was nearly quantitatively converted to σ-dimer **5a-2** through an open-shell intermediate, as indicated by UV−vis−NIR absorption spectroscopy and electron paramagnetic resonance spectroscopy corroborated by spectroscopic calculations, as well as 2D NMR spectra analyses. In situ spectroelectrochemistry was used to confirm the formation process of the dimer radical cation **5a-2**$^{\bullet+}$. Finally, the developed new synthetic strategy could also be applied to obtain π-extended NBN-dibenzoheptazethrene (NBN-DBHZ), representing an efficient pathway toward NBN-doped zigzag-edged graphene nanoribbons.

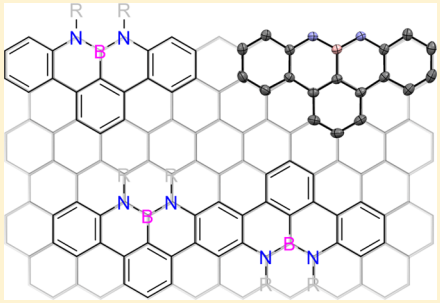

INTRODUCTION

Phenalene (**1**) is the smallest D_{3h}-symmetric polycyclic aromatic hydrocarbon (PAH) with 13 carbon atoms and 13 π electrons. Thus, one electron remains unpaired, rendering this PAH with an open-shell character (Figure 1). Moreover, this compound is a structural motif of nanographenes and graphene nanoribbons (GNRs) that are terminated exclusively by zigzag-edged peripheries.[1] The neutral form of phenalene is a resonance-stabilized radical that can be generated and observed at room temperature in solution,[2] but the study of its optoelectronic properties remains difficult.[3] Inclusion of heteroatoms in the phenalene backbone can strongly influence the chemical and physical properties, as exemplified by 1-azaphenalene (**2**)[4] and 9b-boraphenalene (**3**).[5] Furthermore, the introduction of bilateral benzene rings has been widely used for phenalene derivatives to induce steric shielding of the highly reactive periphery, thus increasing the kinetic stability.[6] We have recently reported that 9a-azaphenalene, which contains a nitrogen atom as a bridgehead within the zigzag-edged periphery, exhibits a stabilized zwitterionic structure similar to that of an azomethine ylide (AMY) with high chemical reactivity.[7]

The implementation of combinations of heteroatoms such as nitrogen and boron, for example, by substituting a C=C unit in an aromatic molecule with an isoelectronic B−N moiety, can significantly affect the electronic structure while leaving the conjugated skeleton unchanged.[8] In addition, in contrast to the nonpolar C=C bond, the B−N bond can also be considered as a zwitterionic double bond in the neutral state, and the oxidation process of the B−N bond has recently received growing interest because of the potential physicochemical properties based on the Lewis acid or base properties of these heteroatoms.[9]

Whereas usually only two carbon atoms are replaced by heteroatoms,[10] more recently the replacement of a full C_3 unit of the zigzag edge with heteroatoms raised interest, allowing the synthesis of stable PAHs with extended zigzag edges. For

Received: April 29, 2016
Published: August 19, 2016

DOI: 10.1021/jacs.6b04445
J. Am. Chem. Soc. 2016, 138, 11606−11615

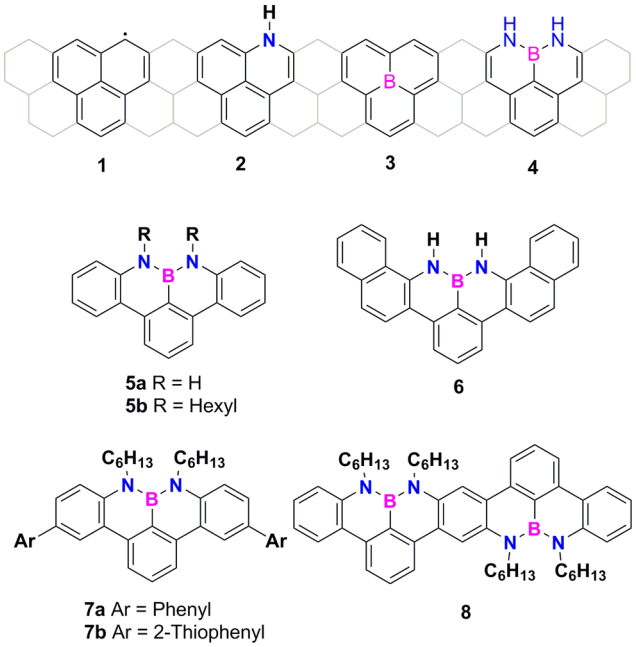

Figure 1. Structures of phenalene (**1**), 1-azaphenalene (**2**), 9b-boraphenalene (**3**), and the unprecedented 1,9-diaza-9a-boraphenalene (**4**). Also shown are the structures of newly synthesized benzo-elongated (**5a** and **5b**), π-extended (**6**), and aryl-substituted (**7a** and **7b**) derivatives as well as the higher homologue **8**.

example, oxygen−boron−oxygen (OBO)-doped double [5]-helicenes with substantial chemical and thermal stabilities were synthesized by Hatakeyama's group and showed excellent ambipolar conductivity.[11] At the same time, our group successfully prepared OBO-doped peritetracenes via cyclo-dehydrogenation of OBO-doped double [5]helicenes,[12] offering the possibility to construct novel heteroatom-doped nanographenes.[13]

In addition to the incorporation of the OBO-doped structure, nitrogen−boron−nitrogen (NBN)-containing aromatic molecules have also raised interest in molecular optoelectronic materials, with the NBN units in most cases restricted to one fused ring.[14] During the preparation of this article, the first example of an NBN-incorporated organic−inorganic hybrid polymer was reported by Helten's group, and its introduction into a PAH with limited π conjugation across the NBN unit was proved.[15]

Here our efforts to understand the effects of heteroatom doping at the zigzag edges of phenalenyl systems on the stability and optoelectronic properties have focused on exploring NBN-incorporated heterophenalenes based on a 1,9-diaza-9a-boraphenalene (**4**) core motif, and in particular, the NBN-doped benzo-elongated phenalene structures **5**−**8** are first reported.[16] Besides, one-electron oxidation of the four-π-electron N−B−N unit could lead to the three-π-electron (N−B−N)* unit, which is isoelectronic to the allylic C−C−C unit, thereby forming an open-shell odd-electron π system, and can provide access to isoelectronic derivatives of the unprecedented full-carbon dibenzophenalenyl radical.

RESULTS AND DISCUSSION

In this work, the syntheses of benzo-elongated zigzag-edged 8*H*,9*H*-8,9-diaza-8a-borabenzo[*fg*]tetracene (**5a**) and its alkylated derivative 8,9-dihexyl-8*H*,9*H*-8,9-diaza-8a-borabenzo[*fg*]-

Scheme 1. Synthesis of NBN-Dibenzophenalene (NBN-DBP) Derivatives

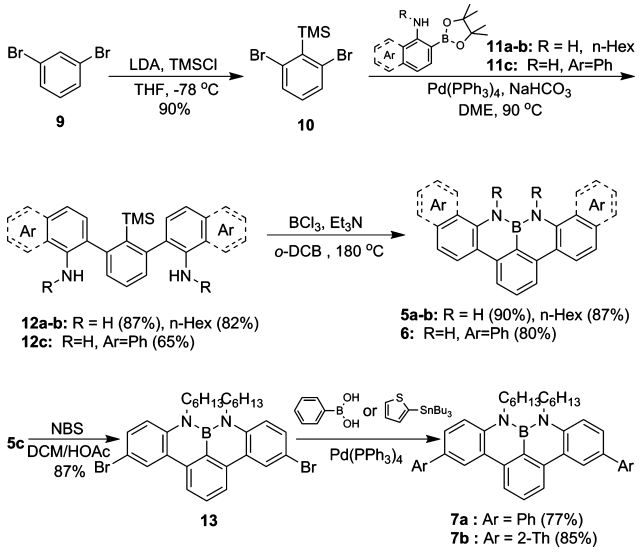

Scheme 2. Synthesis of NBN-Dibenzoheptazethrene (NBN-DBHZ) 8

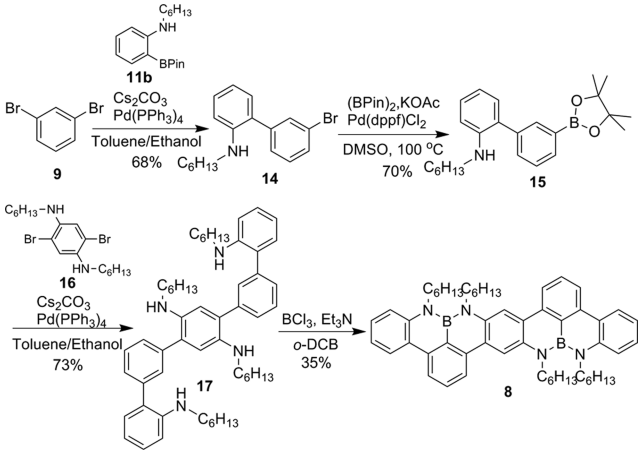

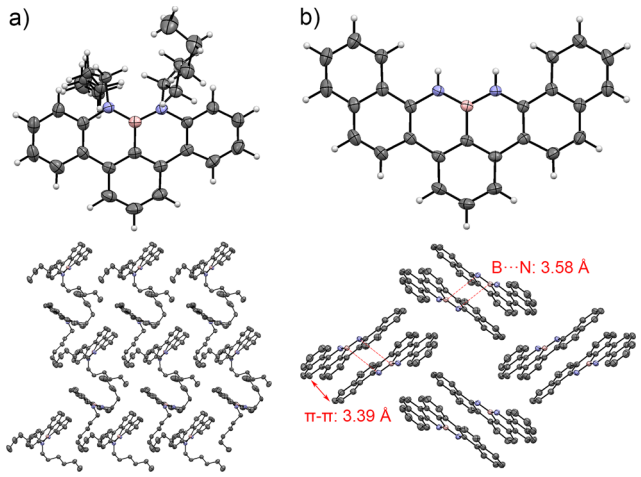

Figure 2. Crystal structures and packing diagrams for (a) **5b** and (b) **6**.

tetracene (**5b**) (also termed dibenzo-fused 1,9-diaza-9a-diboraphenalenes, denoted as NBN-DBPs) were established

DOI: 10.1021/jacs.6b04445
J. Am. Chem. Soc. 2016, 138, 11606−11615

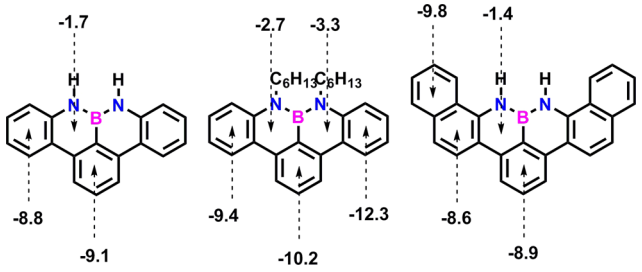

Figure 3. NICS(1) values (in ppm) of compounds **5a**, **5b**, and **6** calculated at the GIAO-B3LYP/6-311+G(2d,p) level. The geometric data for **5b** and **6** were obtained from the crystal structures, and the structure of **5a** was obtained by modifying the structure of **6**.

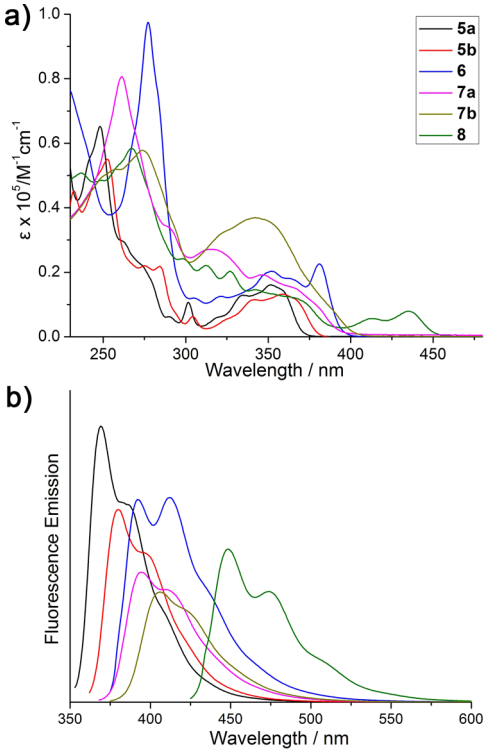

Figure 4. UV−vis absorption spectra (a) and emission spectra (b) of NBN-edged PAHs **5**−**8** at concentrations of 10^{-5} M in CH_2Cl_2.

and further extended to 10,11-dihydro-10,11-diaza-10a-boratribenzo[*a*,*fg*,*l*]tetracene (**6**). The high chemical stability of the zigzag-edged NBN-DBPs allows for an electrophilic bromination process and subsequent derivatization by palladium-catalyzed cross-couplings, as exemplified by 8,9-dihexyl-5,12-diphenyl-8*H*,9*H*-8,9-diaza-8a-borabenzo[*fg*]tetracene (**7a**) and 8,9-dihexyl-5,12-(2-thienyl)-8*H*,9*H*-8,9-diaza-8a-borabenzo[*fg*]tetracene (**7b**). Moreover, 8,9,18,19-tetrahexyl-8*H*,9*H*,18*H*,19*H*-8,9,18,19-tetraaza-8a,18a-diboradibenzo-[a_1b_1,*lm*]heptacene (**8**), which is the next homologue and a diazabora derivative of dibenzoheptazethrene (denoted as NBN-DBHZ), was synthesized to highlight the scope of this solution-based approach toward elongated NBN-edged PAHs. Single-crystal X-ray analyses of compounds **5b**, **6**, and **7a** demonstrated that the B−N bonds have double-bond character. Theoretical, spectroscopic, and electrochemical studies revealed the aromaticity and optoelectronic properties of these unprecedented NBN-edged PAHs. Upon chemical oxidation, as an example, NBN-DBP **5a** was nearly quantitatively

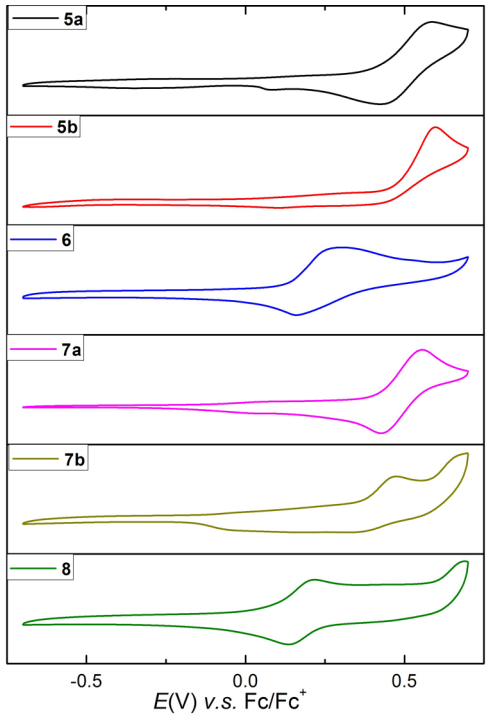

Figure 5. Cyclic voltammograms of NBN-DBPs **5a**−**7b** and NBN-DBHZ **8** measured in CH_2Cl_2 (0.1 mol/L *n*-Bu_4NPF_6) at a scan rate of 100 mV/s. The compounds were scanned for their first oxidation potentials.

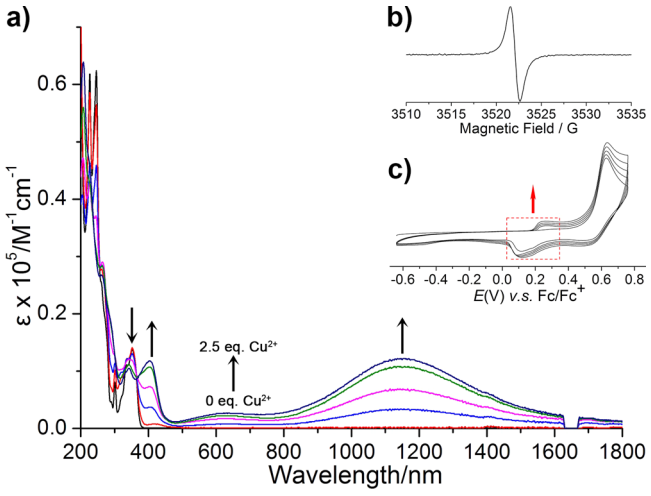

Figure 6. (a) UV−vis−NIR absorption spectra of **5a** titrated with $Cu(OTf)_2$ (0, 0.5, 1.0, 1.5, 2.0, 2.5 equiv) at a concentration of 10^{-5} M in acetonitrile. (b) EPR spectrum of the reaction solution of **5a** + $Cu(OTf)_2$ at 10^{-3} M in acetonitrile. (c) Cyclic voltammograms of **5a** measured in acetonitrile (0.1 mol/L *n*-Bu_4NPF_6) at a scan rate of 100 mV/s.

converted to the σ-dimer **5a-2** through an open-shell intermediate, as indicated by UV−vis−NIR absorption spectroscopy and electron paramagnetic resonance (EPR) spectroscopy corroborated by spectroscopic calculations. The chemical structure of **5a-2** was unambiguously confirmed by two-dimensional (2D) NMR analysis and MALDI-TOF mass spectrometry as the N-para C−C coupling dimer. To gain insight into the radical cations of the NBN-DBPs after single-electron oxidation, we performed in situ spectroelectrochemical

DOI: 10.1021/jacs.6b04445
J. Am. Chem. Soc. 2016, 138, 11606−11615

Table 1. Photochemical and Electrochemical Properties of the NBN-Edged PAHs

	UV−vis absorption			fluorescence		electrochemistry		DFT calculations	
	λ_{abs} [a] (nm)	log ε	E_g [b] (eV)	λ_{em} (nm)	Φ_{PL} [c]	E_{HOMO} [d] (eV)	E_{LUMO} [e] (eV)	IP [f] (eV)	EA [f] (eV)
5a	351	4.21	3.35	369	0.24	−5.31	−1.96	5.63	1.51
5b	359	4.12	3.26	380	0.21	−5.36	−2.10	5.70	1.28
6	381	4.35	3.15	393	0.26	−5.06	−1.91	5.42	1.59
7a	342	4.28	3.15	394	0.19	−5.32	−2.17	5.65	1.34
7b	346	4.57	3.08	406	0.09	−5.26	−2.16	5.61	1.42
8	435	3.90	2.74	448	0.83	−4.99	−2.25	5.32	1.56

[a]Absorption wavelengths of the first absorption maxima. [b]Estimated from the UV−vis absorption edge. [c]Absolute values. [d]Calculated from the onsets of the first oxidation waves using $E_{HOMO} = -E_{ox1} - 4.80$ eV. [e]Estimated according to $E_{LUMO} = E_{HOMO} + E_g$. [f]The polarization- and relaxation-corrected ionization potentials (IP) and electron affinities (EA) correspond to the HOMOs and LUMOs, respectively (see the SI for more details).

Scheme 3. Plausible Oxidation Process of 5a

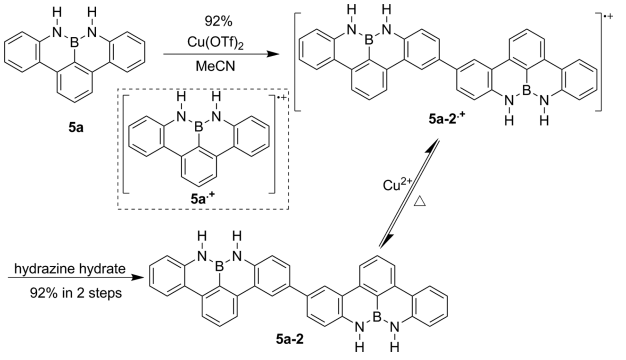

studies of **7a**. The diphenyl substituents at the N-para positions of the NBN-DBP successfully prevented oligomerization and allowed in situ vis−NIR and EPR characterizations of the open-shell radical cation **7a**$^{\bullet+}$. For **7a**$^{\bullet+}$ a large bathochromic shift with a maximum absorption at 1384 nm was observed together with a broad EPR signal at $g = 2.0026$ and a homogeneous spin density distribution over the whole PAH framework.

Synthesis and Structural Characterization. The targeted NBN-DBP derivatives **5a**, **5b**, and **6** were synthesized in three steps, as depicted in Scheme 1. A trimethylsilyl (TMS) group was introduced to act as a directing group during facile twofold electrophilic aromatic borylation, which was used to fuse the N−B−N unit at the perimeter of the PAH in high yield.[17] First, 1,3-dibromobenzene (**9**) was selectively lithiated in the 2-position using lithium diisopropylamide (LDA), and this reaction was quenched with trimethylsilyl chloride to provide 1,3-dibromo-2-(trimethylsilyl)benzene (**10**) in 90% yield.[18] In the second step, palladium-catalyzed Suzuki couplings of **10** with the 2-aminoarylboronic acid esters 2-(4,4,5,5-tetramethyl-1,3,2-dioxaborolan-2-yl)aniline (**11a**), *N*-hexyl-2-(4,4,5,5-tetramethyl-1,3,2-dioxaborolan-2-yl)aniline (**11b**), and 2-(4,4,5,5-tetramethyl-1,3,2-dioxaborolan-2-yl)-naphthalen-1-amine (**11c**) provided the corresponding uncyclized intermediates 2′-(trimethylsilyl)-[1,1′:3′,1″-terphenyl]-2,2″-diamine (**12a**), N^2,$N^{2\prime\prime}$-dihexyl-2′-(trimethylsilyl)-[1,1′:3′,1″-terphenyl]-2,2″-diamine (**12b**), and 2,2′-(2-(trimethylsilyl)-1,3-phenylene)bis(1-aminonaphthalen-2-yl) (**12c**) in yields of 87%, 82%, and 65%, respectively. In the final cyclization step, compounds **12a−c** were treated with BCl_3 and excess triethylamine at 180 °C to furnish the targeted NBN-edged PAHs **5a**, **5b**, and **6** via electrophilic borylation, which was directed by the central TMS group. The crude products were stable enough for purification by column chromatography on silica gel and recrystallization from

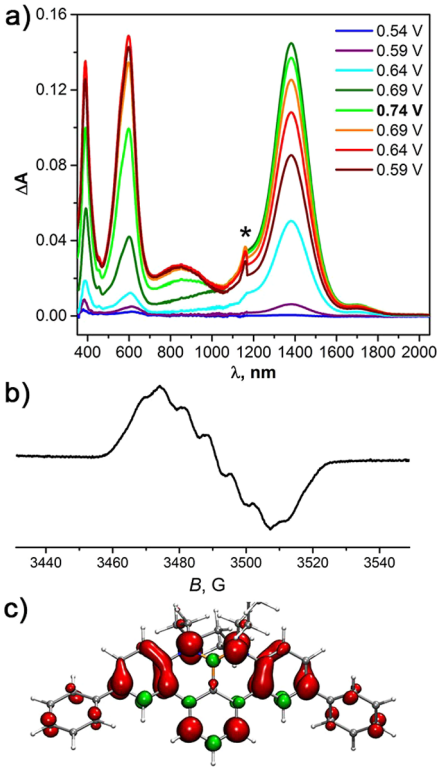

Figure 7. (a) Selected vis−NIR absorption spectra measured in situ during cyclic voltammetry of **7a** at its first oxidation peak. The vertex potential was 0.74 V vs Fc/Fc^+. The asterisk at 1180 nm denotes an artifact of the spectrometer due to the change of detector channels. (b) EPR spectrum of radical cation **7a**$^{\bullet+}$ measured in situ during electrochemical oxidation of **7a** at a potential of 0.59 V. (c) DFT-computed spin density distribution in **7a**$^{\bullet+}$ (red "+", green "−"; alkyl chains have been abridged for clarity).

$CHCl_3$/MeOH to furnish **5a** and **5b** as colorless crystalline solids in 90% and 87% yield, respectively. Recrystallization from THF/MeOH afforded π-extended derivative **6** as a light-green powder in 80% yield.

The stability of the NBN-DBPs allows further modifications of the skeleton that extend the π conjugation and tune the optoelectronic properties of these heteroacenes. Thus, compound **5b** was successfully brominated with 2 equiv of *N*-bromosuccinimide (NBS) to furnish 5,12-dibromo-8,9-dihexyl-8*H*,9*H*-8,9-diaza-8a-borabenzo[*fg*]tetracene (**13**) as a white solid in 87% yield, allowing for further functionalization through palladium-catalyzed cross-coupling reactions. For instance, Suzuki and Stille coupling reactions were performed with **13** to produce π-extended compounds substituted with

DOI: 10.1021/jacs.6b04445
J. Am. Chem. Soc. 2016, 138, 11606−11615

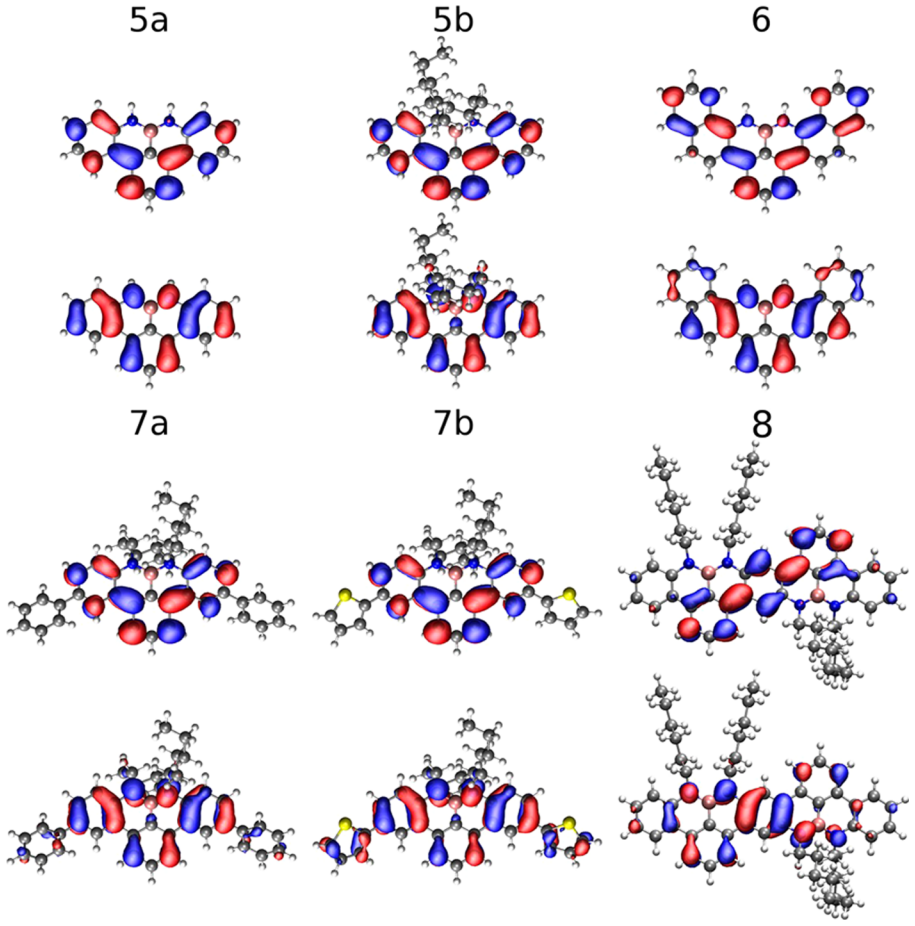

Figure 8. (top) LUMOs and (bottom) HOMOs of NBN-edged PAHs **5a**−**8** obtained from DFT calculations.

phenyl and 2-thienyl moieties (**7a** in 77% yield and **7b** in 85% yield, respectively) as colorless solids.

Inspired by the efficient cyclization protocol, we aimed to synthesize **8**, an NBN-DBHZ containing two 1,9-diaza-9a-boraphenalene motifs (Scheme 2). Because of the decreasing solubility of these larger conjugated systems, we explored the synthesis of NBN-DBHZ **8** from the *N*-alkyl-substituted quinquephenyl precursor $N^2,N^{2''},N^{2''''},N^{5''}$-tetrahexyl-[1,1′:3′,1″:4″,1‴:3‴,1⁗-quinquephenyl]-2,2″,2⁗,5″-tetraamine (**17**). Compound **9** was reacted with 0.5 equiv of boronic acid ester **3b** to furnish the monofunctionalized coupling product 3′-bromo-*N*-hexyl-[1,1′-biphenyl]-2-amine (**14**). This compound was then converted into the corresponding boronic acid ester, *N*-hexyl-3′-(4,4,5,5-tetramethyl-1,3,2-dioxaborolan-2-yl)-[1,1′-biphenyl]-2-amine (**15**), using $Pd(dppf)Cl_2$ as a catalyst. The crude product was purified by flash column chromatography and used immediately for the next palladium-catalyzed reaction. Excess **15** was reacted with 2,5-dibromo-N^1,N^4-dihexylbenzene-1,4-diamine (**16**) to obtain **17** as a yellow oil in 73% yield. Finally, product **17** was treated with BCl_3 and triethylamine at 180 °C to afford pure NBN-DBHZ **8** as a yellow crystalline solid in 35% yield after purification by column chromatography on silica gel and recrystallization from toluene/MeOH.

The intermediates and targeted compounds of NBN-DBPs and NBN-DBHZ were analyzed by ^1H, ^{13}C, and ^{11}B NMR spectroscopy as well as high-resolution mass spectrometry (HRMS). Notably, the broad peak of the amino hydrogen located at around 3.7 ppm in the ^1H NMR spectrum ($CDCl_3$) of intermediate **12a** disappeared after cyclization to target molecule **5a**. For NBN-DBP **5a**, pronounced chemical shifts of protons at the nitrogen sites appeared at about 6.3 ppm, suggesting the aromatic character of BN-fused rings.[19] In the ^1H NMR spectrum ($CDCl_3$) of NBN-DBHZ **8**, there are two groups of triplet resonance peaks at 4.2 and 4.1 ppm which are typically from the methylene protons neighboring the nitrogen, demonstrating the distinction of BN-fused rings in the higher homologue skeleton. In the ^{11}B NMR spectra, all of the NBN-edged PAHs show one broad resonance around 26.7−30.6 ppm, which appears at significantly higher field compared with those of the reported heteroacenes with only BN-embedded structures (35−40 ppm).[20] These NBN-edged PAHs are stable toward ambient oxygen and moisture as solids. They also exhibit good thermal stability with a weight loss of 5% in the range of 250−350 °C based on thermogravimetric analyses (Figure S1 in the Supporting Information (SI)).

X-ray Crystallographic Analysis. Single crystals of compounds **5b** and **7a** suitable for X-ray structure analysis were obtained by slow evaporation of their chloroform solutions. For compound **6** with poorer solubility, suitable crystals were grown by slow evaporation of its THF solution. All of the crystal structures unambiguously reveal the structure of the defined N−B−N zigzag-edged periphery. Compound **5b** shows two types of slightly twisted conformations in one unit cell; the largest dihedral angle of 17.6° is probably due to steric repulsion between the two alkyl chains (Figure 2a). Compound **5b** forms slipped stacks in a herringbone fashion through the many C−H···π interactions formed by the long alkyl chains, but

DOI: 10.1021/jacs.6b04445
J. Am. Chem. Soc. 2016, 138, 11606−11615

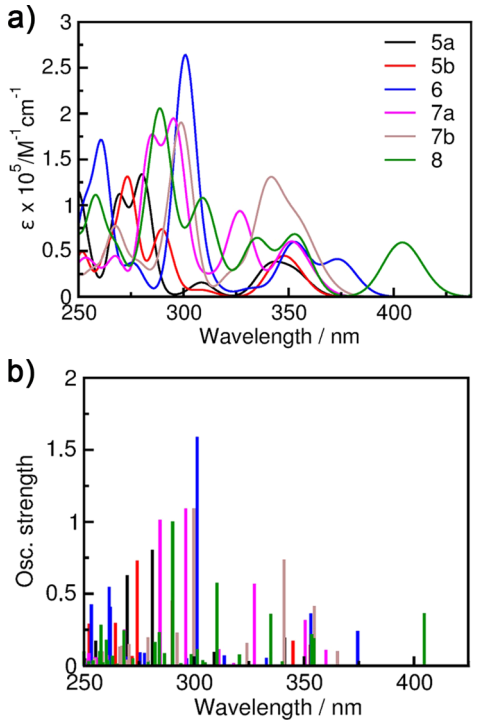

Figure 9. (a) Simulated absorption spectra with Gaussian-type line width broadening (σ = 0.1 eV). (b) Simulated excitation energies and the corresponding oscillator strengths. To reduce a systematic offset relative to the experimental data, a polarization shift to account for solvation effects was applied (see the SI).

no apparent $\pi-\pi$ stacking interactions are observed. The B−N bond lengths in **5b** range from 1.42 to 1.44 Å, which are shorter than the analogous bonds in typical BN-embedded PAHs (1.45−1.47 Å); these data indicate the presence of localized BN double-bond character.[21] Compound **6** exhibits C_{2v} symmetry with an essentially planar backbone; the largest dihedral angle among the fused rings is 2.9°. The two B−N bond lengths in **6** are approximately equivalent to each other at 1.42 Å. The packing diagram of compound **6** reveals a dimeric herringbone motif with intermolecular B−N dipole−dipole interactions at a distance of 3.58 Å, which is below the sum of the van der Waals radii (3.60 Å) (Figure 2b).[22] For compound **7a** (Figure S2), the central core shows a slightly twisted conformation with the largest dihedral angles of 14.4°, similar to the structural characteristics of compound **5b**.

NICS Calculations. To understand how the NBN substitution influences the aromaticity of the dibenzophenalenes, we performed nucleus-independent chemical shift (NICS) calculations at the B3LYP/6-311+G(2d,p) level. As illustrated in Figure 3, the symmetrical NBN-DBP **5a** has a weakly aromatic phenalene core with a small negative NICS(1) value of −1.7 ppm for both BN rings and moderately aromatic features for the fused benzene rings. Similarly, the NICS(1) values for compound **6** are axisymmetric at −1.4 ppm for the BN rings. The peripheral benzene ring has a relatively negative NICS(1) value of −9.8 ppm, revealing more aromaticity than the rings adjacent to the BN core (−8.6 and −8.9 ppm). In contrast, compound **5b** has different NICS(1) values, which may be caused by the steric repulsion between the alkyl chains according to the structural analysis.[23] Notably, the neighboring BN rings in **5b** have stronger aromaticity (−2.7 and −3.3 ppm, respectively) than those of **5a**, which could be explained by the strengthened electron-donating ability of the alkyl chains derived from the polarity of the B−N bonds. The NICS(1) calculation results for the other NBN-edged PAHs **7** and **8** are shown in Figure S3.

Absorption and Emission Spectra. The UV−vis absorption spectra of the as-prepared NBN-edged PAHs are presented in Figure 4a. For NBN-DBPs **5a** and **5b**, two main absorption features are recorded in the wavelength regions of 250−300 and 300−400 nm, with the absorption maxima for the latter at λ = 351 and 359 nm (log ε = 4.21 and 4.12), respectively, which are the wavelengths assigned to the $\pi-\pi^*$ transitions. The intensities of the peaks in the high-energy regions and the red shift (30 nm) of the absorption maximum at λ = 381 nm (log ε = 4.35) for **6** exceeded those of **5a**; these enhancements originate from the extended aromatic skeleton with the additional terminally fused benzene rings.[24] Compounds **7a** and **7b** both exhibit a red-shifted absorption onset and stronger absorption intensity at approximately 300−400 nm compared with **5b**. These results are attributed to the extended π conjugation for **7a** and **7b**, while the absorption maxima are blue-shifted to 342 and 346 nm (log ε = 4.28 and 4.57), respectively. For NBN-DBHZ **8**, the absorption maximum is shifted further to 435 nm (log ε = 3.90). This large bathochromic shift is consistent with the extended conjugation in the higher homologue **8** with its repeated structural motif. The fluorescence of these compounds was also investigated (Figure 4b). Distinct red shifts were found in the emission maxima of the as-prepared NBN-edged PAHs in the following sequence: **5a** (369 nm) < **5b** (380 nm) < **6** (393 nm) < **7a** (394 nm) < **7b** (406 nm) < **8** (448 nm). Notably, NBN-DBHZ **8** exhibits split emission bands at longer wavelengths, and it has a much higher fluorescence quantum yield (Φ_{PL}) (0.83) than smaller homologues **5a**-**7b**.[25]

Electrochemical Properties. The electrochemical behaviors of NBN-DBPs **5a**−**7b** and NBN-DBHZ **8** were investigated by cyclic voltammetry (CV). The compounds were scanned for their first oxidation potentials in CH_2Cl_2, as shown in Figure 5. NBN-DBP **5a** showed a quasi-reversible wave at 0.51 V (vs Fc/Fc^+). The cyclic voltammetry of **5a** was also performed in acetonitrile. Notably, besides an irreversible redox wave at a higher potential, a new reversible redox peak appeared at a lower potential upon multicycle scanning, suggesting the formation of possible oligomers or polymers (Figure 6c), and the follow-up experiments proved the σ-dimer structure (see below).[26] NBN-DBP **5b**, with alkyl substituents on the nitrogen atoms, offered an irreversible peak at 0.60 V. A quasi-reversible peak at 0.25 V was observed for **6**, which is much lower than that for **5a** as a result of the extended π-conjugated skeleton of **6**. Interestingly, **7a** terminated with phenyl substituents at the sides showed an one-electron reversible redox peak at 0.49 V, while **7b** gave an irreversible wave at 0.47 V, probably because of its thiophene terminal groups with electrochemical activity.[27] The first oxidation potentials of **7a** and **7b** are remarkably lower than those of **5a** and **5b**, suggesting that the introduction of aromatic units in the N-para position of such kinds of NBN-DBPs enable extension of the π conjugation., the CV profile of NBN-DBHZ **8** exhibits one quasi-reversible oxidation wave at the lowest potential among these molecules, 0.18 V, as a result of its largest π-conjugated backbone. Obviously, the significant differences in the CV profiles of these compounds are highly associated with their intrinsic molecular structures, and even a tiny variation of these molecular structures would cause a significant change in

DOI: 10.1021/jacs.6b04445
J. Am. Chem. Soc. 2016, 138, 11606−11615

their electrochemical behavior. Accordingly, the highest occupied molecular orbital (HOMO) energy levels of the as-prepared NBN-edged PAHs were evaluated from the onsets of the first oxidation potentials. The low-lying HOMO energy levels of these NBN-DBPs **5** and **7** (−5.26 to −5.36 eV) suggest that these compounds are promising candidates for air-stable p-type semiconductors.[28] Moreover, the lowest unoccupied molecular orbital (LUMO) energy levels were calculated from the HOMO values and the optical band gaps (Table 1).

Chemical Oxidation of NBN-DBPs. Encouraged by the electrochemical behaviors of the NBN-DBPs, we first examined the chemical oxidation of **5a** as a typical example. Given its quasi-reversible redox process with the first oxidation potential of E^1_{ox} = 0.59 V (vs Fc/Fc^+), an exergonic thermal electron transfer (ET) ($\Delta G_{ET} < 0$) to Cu^{2+} to form the radical cation can be predicted.[29] Indeed, titration of **5a** with $Cu(OTf)_2$ resulted in a large bathochromic shift, indicating the formation of radical cation species based on the UV−vis−NIR absorption spectra (Figure 6a).[30] With the progressive addition of $Cu(OTf)_2$, a set of new absorption peaks in the visible and NIR regions of **5a** gradually evolved at 404, 620, and 1150 nm with a concomitant decrease of the $\pi-\pi^*$ transition bands at 336 and 352 nm. A well-defined isosbestic point at 367 nm could be clearly identified. Moreover, upon addition of $Cu(OTf)_2$ in acetonitrile at 10^{-3} M, the EPR spectrum revealed a strong signal at g = 2.0033 with a peak-to-peak width of 1 G (Figure 6b), without any hyperfine coupling observed. This result suggests many different couplings from a highly delocalized structure over which the spin density of the unpaired electron is distributed.[31] Meanwhile, the extremely rapid and distinct change from a colorless solution to a deep-green suspension could also be observed by the naked eye. To exclude the EPR-active interference of Cu, we also used the EPR-inactive oxidant $NOBF_4$ for the oxidation of compound **5a**, and under the same conditions we detected a similar but weaker EPR signal (Figure S4).

In order to gain further insight into these interesting results, the reaction of **5a** with $Cu(OTf)_2$ in acetonitrile was carried out on a preparative scale (Scheme 3). Treatment of **5a** with 2 equiv of $Cu(OTf)_2$ under a nitrogen atmosphere gave a deep-green suspension in the early stage of the reaction, which resembled the UV−vis−NIR and EPR studies of the initial in situ investigation. Afterward, two different workup methods were employed. In the first one, we added excess hydrazine hydrate to the resulting suspension, leading to a color change from deep green to milky white. After filtration, a new compound (denoted as **5a-2**) with good purity was collected as a white powder in a yield of 92% and was first characterized by ^{1}H NMR spectroscopy. In comparison with the observation of only one broad peak at 8.24 ppm with respect to nitrogen protons for **5a**, the ^{1}H NMR spectrum (DMSO-d_6) of **5a-2** showed two broad peaks at 8.30 and 8.34 ppm assignable to the different nitrogen protons on the phenalene scaffold (Figures S5 and S6). On the basis of 2D NMR analyses (pp S35−S49 in the SI), **5a-2** was unambiguously confirmed as the N-para C−C coupling dimer,[32] also in accordance with the results of MALDI-TOF MS analyses. In the other workup method, the deep-green suspension was directly filtered to afford a dark-green powder without the addition of any reductant. The resulting powder was dissolved in DMSO-d_6 as a green solution and was NMR-silent at room temperature, suggesting the existence of an unpaired electron, while after heating for several minutes in air, the green solution was transformed to a colorless one that showed a set of proton signals consistent with that of the neutral dimer **5a-2** (Figure S7). Combined with the well-resolved MALDI-TOF and negative-mode electrospray ionization MS spectra as well as EPR spectra, this confirmed the formation of the radical cation of **5a-2** with an OTf^- counteranion (**5a-2**$^{\bullet+}$·OTf^-) (pp S50 and S55 and Figure S8 in the SI). Therefore, oxidative dimerization of **5a** via an open-shell intermediate is proposed, as shown in Scheme 3. The conversion between the neutral dimer and the dimer radical cation can be smoothly conducted by a simple redox treatment, as validated by cyclic voltammetry and UV−vis−NIR absorption spectroscopy (Figures S9−S12).

Similarly, *N*-alkyl NBN-DBP **5b** also could be nearly quantitatively converted to the dimer **5b-2** as a white powder upon oxidation treatment. The molecular structure of **5b-2** involving the N-para C−C linkage, similar to **5a-2**, was clearly confirmed by ^{1}H and ^{13}C NMR spectra and HR-MALDI-MS analyses. On the contrary, for compound **7a**, the phenyl substituents at the N-para position was expected to block the formation of similar dimers, which indeed was confirmed by MALDI-TOF MS upon chemical oxidation (pp S51−S52 in the SI). Such a result is highly consistent with its aforementioned reversible electrochemical behavior and clearly demonstrates the highly regioselective activity of such kinds of NBN-edged PAHs.

In Situ Spectroelectrochemistry of NBN-DBPs. To understand the formation process of radical cation **5a-2**$^{\bullet+}$ in more detail, we further performed in situ spectroelectrochemistry (SEC) on compound **5a** in acetonitrile. At a low scan rate of 2.5 mV/s, electrochemical oxidation was followed by a chemical reaction that formed a new compound with an oxidation potential near 0.25 V (Figure S13). In situ EPR/vis−NIR SEC studies showed that oxidation of **5a** in acetonitrile caused the appearance of an absorption band at 1100 nm accompanied by a relatively narrow EPR signal at g = 2.0027 with a line width of 0.7 G. These spectroscopic features are similar to those observed for the solution of the precipitate formed during chemical oxidation of **5a** by Cu^{2+} as discussed in the previous section. In addition, the oxidation potential of the dimer **5a-2** coincides with the oxidation potential of the follow-up products of the electrochemical oxidation of **5a** (Figure S14). These results thus enable us to conclude that the precipitate observed in the chemical oxidation of **5a** is the radical cation **5a-2**$^{\bullet+}$ (see the detailed structure in Figure S15). The SEC studies also showed that the absorption intensity at 1100 nm increased almost 2-fold at the second voltammetric cycle, and the formation of a film was observed on the electrode after the measurements. Presumably, **5a** not only dimerized upon electrochemical oxidation but underwent a further electropolymerization.

For comparison, we also peformed the in situ SEC studies on NBN-DBP **7a**. Obviously, the phenyl substitutions at the N-para positions (which are dimerization sites in **5a**) prevent dimerization/polymerization of **7a**. In situ EPR/vis−NIR measurements during electrochemical oxidation revealed absorption bands of the **7a**$^{\bullet+}$ radical cation at 598 and 1380 nm and a broad EPR signal at g = 2.0026 with the sign of hyperfine structure (Figures 7a,b and S16). Density functional theory (DFT) computations were then conducted with the ORCA package at the B3LYP level using the def2-TZVP basis set for C and the specially tailored EPR-III basis set for H, N, and B, and we found that the spin density in **7a**$^{\bullet+}$ is delocalized

DOI: 10.1021/jacs.6b04445
J. Am. Chem. Soc. 2016, 138, 11606−11615

over the whole π system (Figure 7c), which results in relatively large hyperfine coupling constants (hfcc's) for many nuclei. In particular, the largest hfcc values are predicted for B (−13.5 MHz), one of the protons in the CH_2 groups next to the atoms of nitrogen (16.0 and 18.0 MHz), N (2 × 9.9 MHz), and two protons at the 4,6-diazaboraphenalene positions (2 × −8.3 MHz). The hfcc values for other protons are less than 3 MHz (Figure S17). A combination of many magnetic nuclei with a broad distribution of hfcc values gives a broad EPR signal with a rich hyperfine structure, which cannot be fully resolved.

Spectroscopic Calculations. We further performed DFT calculations using the Gaussian 09 software package[33] at the M06-2X/cc-pVTZ level[34] to characterize the electronic structures of all of the NBN-DBPs and their absorption spectra, as shown in Table 1 and Figures 8 and 9 (see the SI for more details). For all of the molecules except compound **6**, the HOMO (LUMO) frontier orbital is separated by more than 0.4 eV from the lower (higher) energy levels. For compound **6**, the LUMO and LUMO+1 are close, with an energy separation of 0.14 eV. The frontier orbitals of compounds **5a**, **5b**, **6**, **7a**, and **7b** have similar shapes and exhibit a nodal structure that keeps the boron atom clear of weight (Figure 8). The HOMO is partially localized at the nitrogen atoms, while the LUMOs have no weight at that point. For compound **6** the frontier molecular orbitals are even more strongly delocalized over the entire molecule, leading to a reduced ionization potential (IP), a smaller energy gap, and a further red shift in the absorption spectrum (Figure 9), remaining consistent with the experimental CV and UV−vis results. The dominant absorption peak doublet above 350 nm is caused by the energetic proximity of the LUMO and LUMO+1 levels, which are both involved in the electronic transitions. Frontier MOs with greater π delocalization are observed in NBN-DBHZ **8**, leading to a further decrease in the HOMO−LUMO gap and a red shift in the absorption, in agreement with the UV−vis results. Functionalizing **5b** to obtain **7a** and **7b** increases the absorption intensity, while the IP and electron affinity (EA) values and absorption onsets are almost unchanged, corroborating our experimental observations. In addition, we found that the simulated absorption spectra of **5a-2** in various oxidation forms also showed strong absorption in the NIR region similar to the experimental findings, consistent with the reaction of the **5a** monomer to form the **5a-2** dimer structure (Figures S18−20; see the detailed discussion in the SI).

CONCLUSIONS

A synthetic route toward unprecedented heteroatom-doped PAHs featuring a nitrogen−boron−nitrogen-type zigzag-edged periphery based on a 1,9-diaza-9a-boraphenalene core structure was introduced. Alternating nitrogen and boron atoms impart high chemical stability to these zigzag-edged PAHs; this motif even allows for postsynthetic modifications. The possibilities for lateral extension were demonstrated by the synthesis of the higher homologue **8**, suggesting that NBN-doped zigzag-edged graphene nanoribbons could be synthesized via this route.[35] Upon chemical oxidation, as an example, NBN-DBP **5a** was nearly quantitatively converted to the N-para C−C-linked dimer **5a-2** through an open-shell intermediate, revealing the highly regioselective activation of NBN-DBPs at their molecular peripheries. The additional phenyl substituents in **7a** prevented oligomerization, and the clean single-electron oxidation of the NBN unit into the isoelectronic allyl radical could be performed by means of in situ spectroelectrochemistry, generating radical cation $\mathbf{7a}^{\bullet+}$, which is isoelectronic to the unprecedented full-carbon dibenzophenalenyl radical. This work provides a new class of PAH molecules with tunable properties while promoting our strategy to obtain tailor-made complex architectures such as conjugated polymers,[36] dendrimers,[37] organic framework materials,[38] and graphene nanoribbons[39] with stable NBN-doped zigzag-edged peripheries.

ASSOCIATED CONTENT

Supporting Information

The Supporting Information is available free of charge on the ACS Publications website at DOI: 10.1021/jacs.6b04445.

Experimental details, TGA spectra, single-crystal X-ray diffraction data, in situ SEC results, computational details, NMR spectra, and HRMS spectra (PDF)
Crystallographic data for **5b** (CIF)
Crystallographic data for **6** (CIF)
Crystallographic data for **7a** (CIF)

AUTHOR INFORMATION

Corresponding Authors

*fan-zhang@sjtu.edu.cn
*xinliang.feng@tu-dresden.de

Notes

The authors declare no competing financial interest.

ACKNOWLEDGMENTS

We are grateful for the financial supported from the National Basic Research Program of China (973 Program) (2013CBA01602 and 2012CB933404), the National Natural Science Foundation of China (21574080), and the Shanghai Committee of Science and Technology (15JC1490500). The work was partly supported by the German Research Foundation (DFG) through projects EXC 1056 and OR 349/1. Computational resources were provided by the Center for Information Services and High Performance Computing (ZIH) of TU Dresden.

REFERENCES

(1) (a) Morita, Y.; Suzuki, S.; Sato, K.; Takui, T. *Nat. Chem.* **2011**, *3*, 197. (b) Li, Y.; Heng, W.-K.; Lee, B. S.; Aratani, N.; Zafra, J. L.; Bao, N.; Lee, R.; Sung, Y. M.; Sun, Z.; Huang, K.-W.; Webster, R. D.; López Navarrete, J. T.; Kim, D.; Osuka, A.; Casado, J.; Ding, J.; Wu, J. *J. Am. Chem. Soc.* **2012**, *134*, 14913. (c) Li, Y.; Huang, K.-W.; Sun, Z.; Webster, R. D.; Zeng, Z.; Zeng, W.; Chi, C.; Furukawa, K.; Wu, J. *Chem. Sci.* **2014**, *5*, 1908. (d) Ruffieux, P.; Wang, S.; Yang, B.; Sánchez-Sánchez, C.; Liu, J.; Dienel, T.; Talirz, L.; Shinde, P.; Pignedoli, C. A.; Passerone, D.; Dumslaff, T.; Feng, X.; Müllen, K.; Fasel, R. *Nature* **2016**, *531*, 489.

(2) Goto, K.; Kubo, T.; Yamamoto, K.; Nakasuji, K.; Sato, K.; Shiomi, D.; Takui, T.; Kubota, M.; Kobayashi, T.; Yakusi, K.; Ouyang, J. *J. Am. Chem. Soc.* **1999**, *121*, 1619.

(3) (a) Cofino, W. P.; van Dam, S. M.; Kamminga, D. A.; Hoornweg, G. P.; Gooijer, C.; MacLean, C.; Velthorst, N. H. *Mol. Phys.* **1984**, *51*, 537. (b) O'Connor, G. D.; Troy, T. P.; Roberts, D. A.; Chalyavi, N.; Fückel, B.; Crossley, M. J.; Nauta, K.; Stanton, J. F.; Schmidt, T. W. *J. Am. Chem. Soc.* **2011**, *133*, 14554.

(4) O'Brien, S.; Smith, D. C. C. *J. Chem. Soc.* **1963**, 2907.

(5) Rotermund, G. W.; Köster, R. *Justus Liebigs Annalen der Chemie* **1965**, *686*, 153.

(6) Clar, E.; Fell, G. S.; Richmond, M. H. *Tetrahedron* **1960**, *9*, 96.

(7) (a) Berger, R.; Giannakopoulos, A.; Ravat, P.; Wagner, M.; Beljonne, D.; Feng, X.; Müllen, K. *Angew. Chem., Int. Ed.* **2014**, *53*,

DOI: 10.1021/jacs.6b04445
J. Am. Chem. Soc. 2016, 138, 11606−11615

10520. (b) Berger, R.; Wagner, M.; Feng, X.; Müllen, K. *Chem. Sci.* **2015**, *6*, 436.
(8) (a) Liu, Z.; Marder, T. B. *Angew. Chem., Int. Ed.* **2008**, *47*, 242. (b) Bosdet, M. J. D.; Piers, W. E. *Can. J. Chem.* **2009**, *87*, 8. (c) Campbell, P. G.; Marwitz, A. J. V.; Liu, S.-Y. *Angew. Chem., Int. Ed.* **2012**, *51*, 6074. (d) Wang, X.-Y.; Wang, J. Y.; Pei, J. *Chem. - Eur. J.* **2015**, *21*, 3528.
(9) (a) Aramaki, Y.; Omiya, H.; Yamashita, M.; Nakabayashi, K.; Ohkoshi, S.-i.; Nozaki, K. *J. Am. Chem. Soc.* **2012**, *134*, 19989. (b) Suzuki, S.; Yoshida, K.; Kozaki, M.; Okada, K. *Angew. Chem., Int. Ed.* **2013**, *52*, 2499. (c) Rosenthal, A. J.; Devillard, M.; Miqueu, K.; Bouhadir, G.; Bourissou, D. *Angew. Chem., Int. Ed.* **2015**, *54*, 9198.
(10) (a) Agou, T.; Kobayashi, J.; Kawashima, T. *Org. Lett.* **2006**, *8*, 2241. (b) Li, G.; Wu, Y.; Gao, J.; Wang, C.; Li, J.; Zhang, H.; Zhao, Y.; Zhao, Y.; Zhang, Q. *J. Am. Chem. Soc.* **2012**, *134*, 20298. (c) Dou, C. D.; Saito, S.; Matsuo, K.; Hisaki, I.; Yamaguchi, S. *Angew. Chem., Int. Ed.* **2012**, *51*, 12206. (d) Neue, B.; Araneda, J. F.; Piers, W. E.; Parvez, M. *Angew. Chem., Int. Ed.* **2013**, *52*, 9966. (e) Tang, R.; Zhang, F.; Fu, Y.; Xu, Q.; Wang, X.; Zhuang, X.; Wu, D.; Giannakopoulos, A.; Beljonne, D.; Feng, X. *Org. Lett.* **2014**, *16*, 4726.
(11) (a) Sumida, Y.; Harada, R.; Kato-Sumida, T.; Johmoto, K.; Uekusa, H.; Hosoya, T. *Org. Lett.* **2014**, *16*, 6240. (b) Katayama, T.; Nakatsuka, S.; Hirai, H.; Yasuda, N.; Kumar, J.; Kawai, T.; Hatakeyama, T. *J. Am. Chem. Soc.* **2016**, *138*, 5210.
(12) Wang, X.-Y.; Narita, A.; Zhang, W.; Feng, X.; Müllen, K. *J. Am. Chem. Soc.* **2016**, *138*, 9021.
(13) Narita, A.; Wang, X. Y.; Feng, X.; Müllen, K. *Chem. Soc. Rev.* **2015**, *44*, 6616.
(14) (a) Riehm, T.; De Paoli, G.; Wadepohl, H.; De Cola, L.; Gade, L. H. *Chem. Commun.* **2008**, *42*, 5348. (b) Nishida, J.-i.; Fujita, T.; Fujisaki, Y.; Tokito, S.; Yamashita, Y. *J. Mater. Chem.* **2011**, *21*, 16442. (c) Abbey, E. R.; Liu, S.-Y. *Org. Biomol. Chem.* **2013**, *11*, 2060.
(15) Lorenz, T.; Lik, A.; Plamper, F. A.; Helten, H. *Angew. Chem., Int. Ed.* **2016**, *55*, 7236.
(16) During the preparation of this article, Hatakeyama and co-workers reported the synthesis of an *N*-methylic NBN-DBP via demethylative direct borylation. See: Numano, M.; Nagami, N.; Nakatsuka, S.; Katayama, T.; Nakajima, K.; Tatsumi, S.; Yasuda, N.; Hatakeyama, T. *Chem. - Eur. J.* **2016**, *22*, 11574.
(17) Wang, X.; Zhang, F.; Gao, J.; Fu, Y.; Zhao, W.; Tang, R.; Zhang, W.; Zhuang, X.; Feng, X. *J. Org. Chem.* **2015**, *80*, 10127.
(18) Mongin, F.; Marzi, E.; Schlosser, M. *Eur. J. Org. Chem.* **2001**, *2001*, 2771.
(19) (a) Wang, X.; Zhang, F.; Liu, J.; Tang, R.; Fu, Y.; Wu, D.; Xu, Q.; Zhuang, X.; He, G.; Feng, X. *Org. Lett.* **2013**, *15*, 5714. (b) Wang, X.-Y.; Zhuang, F.-D.; Wang, X.-C.; Cao, X.-Y.; Wang, J.-Y.; Pei, J. *Chem. Commun.* **2015**, *51*, 4368.
(20) (a) Wang, X.-Y.; Lin, H. R.; Lei, T.; Yang, D. C.; Zhuang, F. D.; Wang, J. Y.; Yuan, S. C.; Pei, J. *Angew. Chem., Int. Ed.* **2013**, *52*, 3117. (b) Wang, X.-Y.; Zhuang, F.-D.; Wang, R.-B.; Wang, X.-C.; Cao, X.-Y.; Wang, J.-Y.; Pei, J. *J. Am. Chem. Soc.* **2014**, *136*, 3764. (c) Ishibashi, J. S.; Marshall, J. L.; Maziere, A.; Lovinger, G. J.; Li, B.; Zakharov, L. N.; Dargelos, A.; Graciaa, A.; Chrostowska, A.; Liu, S.-Y. *J. Am. Chem. Soc.* **2014**, *136*, 15414.
(21) (a) Lepeltier, M.; Lukoyanova, O.; Jacobson, A.; Jeeva, S.; Perepichka, D. F. *Chem. Commun.* **2010**, *46*, 7007. (b) Hatakeyama, T.; Hashimoto, S.; Seki, S.; Nakamura, M. *J. Am. Chem. Soc.* **2011**, *133*, 18614. (c) Müller, M.; Maichle-Mossmer, C.; Bettinger, H. F. *Angew. Chem., Int. Ed.* **2014**, *53*, 9380.
(22) Jaska, C. A.; Emslie, D. J. H.; Bosdet, M. J. D.; Piers, W. E.; Sorensen, T. S.; Parvez, M. *J. Am. Chem. Soc.* **2006**, *128*, 10885.
(23) Schaffroth, M.; Gershoni-Poranne, R.; Stanger, A.; Bunz, U. H. F. *J. Org. Chem.* **2014**, *79*, 11644.
(24) (a) Niimi, K.; Shinamura, S.; Osaka, I.; Miyazaki, E.; Takimiya, K. *J. Am. Chem. Soc.* **2011**, *133*, 8732. (b) Mori, T.; Nishimura, T.; Yamamoto, T.; Doi, I.; Miyazaki, E.; Osaka, I.; Takimiya, K. *J. Am. Chem. Soc.* **2013**, *135*, 13900.
(25) Wetzel, C.; Brier, E.; Vogt, A.; Mishra, A.; Mena-Osteritz, E.; Bäuerle, P. *Angew. Chem., Int. Ed.* **2015**, *54*, 12334.
(26) (a) Smie, A.; Heinze, J. *Angew. Chem., Int. Ed. Engl.* **1997**, *36*, 363. (b) Heinze, J.; Willmann, C.; Bäuerle, P. *Angew. Chem., Int. Ed.* **2001**, *40*, 2861. (c) Chen, X.; Wang, X.; Zhou, Z.; Li, Y.; Sui, Y.; Ma, J.; Wang, X.; Power, P. P. *Angew. Chem., Int. Ed.* **2013**, *52*, 589.
(27) (a) Waltman, R. J.; Diaz, A. F.; Bargon, J. *J. Phys. Chem.* **1984**, *88*, 4343. (b) Roncali, J. *Chem. Rev.* **1992**, *92*, 711. (c) Lukoyanova, O.; Lepeltier, M.; Laferrière, M.; Perepichka, D. F. *Macromolecules* **2011**, *44*, 4729.
(28) (a) Gao, J. H.; Li, R. J.; Li, L. Q.; Meng, Q.; Jiang, H.; Li, H. X.; Hu, W. P. *Adv. Mater.* **2007**, *19*, 3008. (b) Wang, C.; Dong, H.; Hu, W.; Liu, Y.; Zhu, D. *Chem. Rev.* **2012**, *112*, 2208.
(29) The redox potential of the Cu^{2+}−Cu^{+} couple was estimated to be +0.65 V vs Fc^{+}−Fc. See: (a) Cox, B. G.; Jedral, W.; Palou. *J. Chem. Soc., Dalton Trans.* **1988**, *3*, 733. (b) Connelly, N. G.; Geiger, W. E. *Chem. Rev.* **1996**, *96*, 877.
(30) (a) Ajayakumar, M.; Asthana, D.; Mukhopadhyay, P. *Org. Lett.* **2012**, *14*, 4822. (b) Wu, X.; Guo, Z.; Wu, Y.; Zhu, S.; James, T. D.; Zhu, W. *ACS Appl. Mater. Interfaces* **2013**, *5*, 12215. (c) Jung, J. Y.; Kang, M.; Chun, J.; Lee, J.; Kim, J.; Kim, J.; Kim, Y.; Kim, S.-J.; Lee, C.; Yoon, J. *Chem. Commun.* **2013**, *49*, 176.
(31) Ji, L.; Edkins, R. M.; Lorbach, A.; Krummenacher, I.; Brückner, C.; Eichhorn, A.; Braunschweig, H.; Engels, B.; Low, P. J.; Marder, T. B. *J. Am. Chem. Soc.* **2015**, *137*, 6750.
(32) For examples of N-para σ dimers, see: (a) Kamada, K.; Fuku-en, S.-i.; Minamide, S.; Ohta, K.; Kishi, R.; Nakano, M.; Matsuzaki, H.; Okamoto, H.; Higashikawa, H.; Inoue, K.; Kojima, S.; Yamamoto, Y. *J. Am. Chem. Soc.* **2013**, *135*, 232. (b) Zheng, X.; Wang, X.; Qiu, Y.; Li, Y.; Zhou, C.; Sui, Y.; Li, Y.; Ma, J.; Wang, X. *J. Am. Chem. Soc.* **2013**, *135*, 14912. For biphenalenylidene examples, see: (c) Uchida, K.; Ito, S.; Nakano, M.; Abe, M.; Kubo, T. *J. Am. Chem. Soc.* **2016**, *138*, 2399. (d) Uchida, K.; Mou, Z.; Kertesz, M.; Kubo, T. *J. Am. Chem. Soc.* **2016**, *138*, 4665.
(33) Frisch, M. J.; Trucks, G. W.; Schlegel, H. B.; Scuseria, G. E.; Robb, M. A.; Cheeseman, J. R.; Scalmani, G.; Barone, V.; Mennucci, B.; Petersson, G. A.; Nakatsuji, H.; Caricato, M.; Li, X.; Hratchian, H. P.; Izmaylov, A. F.; Bloino, J.; Zheng, G.; Sonnenberg, J. L.; Hada, M.; Ehara, M.; Toyota, K.; Fukuda, R.; Hasegawa, J.; Ishida, M.; Nakajima, T.; Honda, Y.; Kitao, O.; Nakai, H.; Vreven, T.; Montgomery, J. A., Jr.; Peralta, J. E.; Ogliaro, F.; Bearpark, M.; Heyd, J. J.; Brothers, E.; Kudin, K. N.; Staroverov, V. N.; Kobayashi, R.; Normand, J.; Raghavachari, K.; Rendell, A.; Burant, J. C.; Iyengar, S. S.; Tomasi, J.; Cossi, M.; Rega, N.; Millam, J. M.; Klene, M.; Knox, J. E.; Cross, J. B.; Bakken, V.; Adamo, C.; Jaramillo, J.; Gomperts, R.; Stratmann, R. E.; Yazyev, O.; Austin, A. J.; Cammi, R.; Pomelli, C.; Ochterski, J. W.; Martin, R. L.; Morokuma, K.; Zakrzewski, V. G.; Voth, G. A.; Salvador, P.; Dannenberg, J. J.; Dapprich, S.; Daniels, A. D.; Farkas, Ö.; Foresman, J. B.; Ortiz, J. V.; Cioslowski, J.; Fox, D. J. *Gaussian 09*, revision D.01; Gaussian, Inc.: Wallingford, CT, 2009.
(34) (a) Zhao, Y.; Truhlar, D. G. *Theor. Chem. Acc.* **2008**, *120*, 215. (b) Dunning, T. H. *J. Chem. Phys.* **1989**, *90*, 1007. (c) Kendall, R. A.; Dunning, T. H.; Harrison, R. J. *J. Chem. Phys.* **1992**, *96*, 6796.
(35) (a) Narita, A.; Feng, X.; Hernandez, Y.; Jensen, S. A.; Bonn, M.; Yang, H.; Verzhbitskiy, I. A.; Casiraghi, C.; Hansen, M. R.; Koch, A. H. R.; Fytas, G.; Ivasenko, O.; Li, B.; Mali, K. S.; Balandina, T.; Mahesh, S.; De Feyter, S.; Müllen, K. *Nat. Chem.* **2014**, *6*, 126. (b) Bunz, U. H. F. *Acc. Chem. Res.* **2015**, *48*, 1676.
(36) (a) Jäkle, F. *Chem. Rev.* **2010**, *110*, 3985. (b) Lei, T.; Wang, J.-Y.; Pei, J. *Acc. Chem. Res.* **2014**, *47*, 1117. (c) Baggett, A. W.; Guo, F.; Li, B.; Liu, S.-Y.; Jäkle, F. *Angew. Chem., Int. Ed.* **2015**, *54*, 11191.
(37) (a) Vögtle, F.; Gestermann, S.; Hesse, R.; Schwierz, H.; Windisch, B. *Prog. Polym. Sci.* **2000**, *25*, 987. (b) Hammer, B. A. G.; Moritz, R.; Stangenberg, R.; Baumgarten, M.; Müllen, K. *Chem. Soc. Rev.* **2015**, *44*, 4072.
(38) (a) Feng, X.; Ding, X.; Jiang, D. *Chem. Soc. Rev.* **2012**, *41*, 6010. (b) Kawasumi, K.; Zhang, Q.; Segawa, Y.; Scott, L. T.; Itami, K. *Nat. Chem.* **2013**, *5*, 739. (c) Sánchez-Sánchez, C.; Brüller, S.; Sachdev, H.; Müllen, K.; Krieg, M.; Bettinger, H. F.; Nicolaï, A.; Meunier, V.; Talirz, L.; Fasel, R.; Ruffieux, P. *ACS Nano* **2015**, *9*, 9228.

DOI: 10.1021/jacs.6b04445
J. Am. Chem. Soc. 2016, 138, 11606−11615

(39) (a) Son, Y.-W.; Cohen, M. L.; Louie, S. G. *Nature* **2006**, *444*, 347. (b) Cai, J.; Ruffieux, P.; Jaafar, R.; Bieri, M.; Braun, T.; Blankenburg, S.; Muoth, M.; Seitsonen, A. P.; Saleh, M.; Feng, X.; Müllen, K.; Fasel, R. *Nature* **2010**, *466*, 470.

DOI: 10.1021/jacs.6b04445
J. Am. Chem. Soc. 2016, 138, 11606−11615